IEEE Access
Multidisciplinary ⋮ Rapid Review ⋮ Open Access Journal

Received July 2, 2021, accepted July 18, 2021, date of publication August 24, 2021, date of current version September 17, 2021.

Digital Object Identifier 10.1109/ACCESS.2021.3107055

Size-Reduction of a Dual-Band Circularly Polarized Dielectric Resonator Antenna

AMIR ALTAF, (Member, IEEE), AND MUNKYO SEO, (Senior Member, IEEE)
Department of Electrical and Computer Engineering, Sungkyunkwan University, Suwon 440-746, South Korea

Corresponding author: Munkyo Seo (mkseo@skku.edu)

This work was supported by the Institute of Information & communications Technology Planning & Evaluation (IITP) Grant funded by the Korean Government (MSIT) (Development of key technologies for 6G RF front-end based on low-power MIMO and highly efficient spatial QAM synthesis) under Grant 2021-0-00198.

ABSTRACT In this paper, the size reduction of a dual-band circularly polarized (CP) Y-shaped dielectric resonator antenna (YDRA) is performed. Unlike the conventional CP DRAs, the circular polarization in the YDRA is achieved by the combination of linearly varying E-fields in the two arms of unequal length. Therefore, a PEC boundary condition based technique is applied to the long arm of the dielectric resonator (DR). As a result, a 33.18% reduction in the size is achieved after the optimization of the DR for the required frequency bands. A sample of the proposed design is fabricated to perform measurements. From the results, the antenna obtains a wide impedance bandwidth for $|S_{11}| \leq -10$ dB of 53.5% (2.3–3.98 GHz), 3 dB axial ratios bandwidths (ARBWs) of 4.08% (2.4–2.50 GHz) and 10.91% (3.38–3.77 GHz) with respective peak gains of 4.83 dBic and 4.81 dBic. The attained 3 dB ARBWs entirely cover the WLAN 2.4 GHz and WiMAX 3.5 GHz frequency bands.

INDEX TERMS Circular polarization, dielectric resonator antenna (DRA), miniaturization, PEC boundary.

I. INTRODUCTION

In early 1983, Long *et al*. pioneered the field of ceramic antennas after studying the resonant modes, radiation characteristics and excitation of modes in the cylindrical dielectric resonator (CDR) [1]. McAllister and Long also presented the rectangular and hemispherical dielectric resonator antennas (DRAs) in the same and following year, respectively [2], [3]. In the aftermath, the DRAs have been researched for various characteristics such as wide bandwidth, high gain, pattern, and polarization reconfigurability to name a few. The benefits of employing DRAs as compared to metallic antennas are the relatively wider bandwidth, and higher radiation efficiency that is primarily attributed to the absence of conductor losses.

Due to the recent advancement in wireless communication, the requirement of dual-/wide-band antennas has also increased. For such systems, integration of circularly polarized (CP) DRAs will enhance the performance as these antennas are unaffected by the orientation of the transmitter (Tx) and receiver and perform well against multi-path interference or fading. One way to design a CP DRA is the selection of an appropriate feeding mechanism (FM). The dual-point-based FM demonstrates a wider 3 dB axial ratio bandwidth (ARBW) but takes up more space [4]–[6]. The single-point type FM is simpler but typically obtains a narrow 3 dB ARBW [7]–[9]. The other strategy relies on the shape modification of the DR [10]–[16]. Recently, the combination of singly-feeding technique and modified DRs have been reported to achieve wider 3 dB ARBWs that are comparable with dual-point fed DRAs [17]–[19]. For instance, a cut in the rectangular DR (RDR) followed by the addition of a smaller ceramic block achieved a wide 3 dB ARBW of 44.73% [17]. In [18], a fan-blade-shaped CP DRA produces a dual-band response with 3 dB ARBWs of 13.33% and 7.81%. Similarly, a sigmoid-shaped dual-band CP DRA is reported with 3 dB ARBWs of 19.98% and 3.07% [19].

The development of compact dual-/wide-band antennas is of great importance for portable device applications. For microstrip antennas, various methods such as defected ground structure (DGS), reactive loading, meandered and fractal geometries have been demonstrated to achieve miniaturization but at the expense of radiation property [20]. DRAs being efficient radiators have also been explored in this context. The applied miniaturization methods can be classified into five categories that are (i) use of the high dielectric material, (ii) application of boundary conditions

The associate editor coordinating the review of this manuscript and approving it for publication was Debabrata Karmokar.

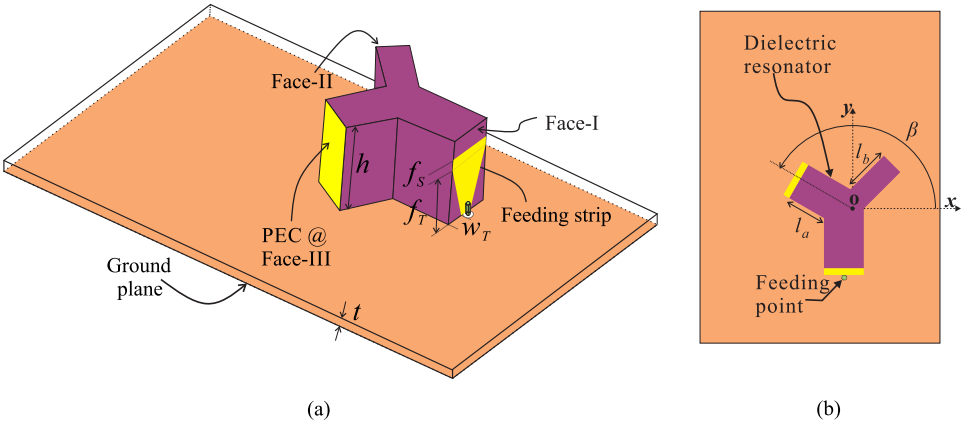

FIGURE 1. Geometry of the miniaturized DRA. (a) Panoramic view. (b) Top view. $[h = 21.7, f_T = 13.32, f_S = 1.48, w_T = 4.8, l_a = 12.73, l_b = 13.25.]_{mm}$, $[\beta = 150°]$.

(PEC/PMC), (iii) loading the metallic strips around or top or both surfaces of the DR, (iv) application of artificial magnetic conductor (AMC), and (v) use of slot with meander lines. One example of the first method uses a high permittivity ($\varepsilon_r = 100$) material but archives a narrow -10 dB impedance bandwidth (IBW) of 3% [21]. Another work proposed a two-segment DR with a high aspect ratio to simultaneously achieve miniaturization and -10 dB IBW > 11% [22]. For (ii), the volume of DR was reduced by 50% by placing the PEC at the symmetry [23], [24]. A combination of PEC and PMC boundary conditions reduced the size by 75% [24]. Recently, a dielectric patch of very high permittivity is utilized as a PEC resulting in a size reduction of one-half [25]. The works [26]–[28] belong to the third category where miniaturization is achieved by covering only the top surface, two surfaces (top and front wall), and three surfaces (left, right, and front) with metallic strips but produces a narrow bandwidth. For category (iv), Shahid *et al.* proposed the DRA with AMC to achieve miniaturization with a narrow bandwidth [29] and for (v), a work is reported recently [30]. However, all the above methods are mainly applied to linearly polarized radiators and yield a single narrow-band response. Therefore DRAs that can simultaneously deliver the dual-/wide-band -10 dB IBW, miniaturization, and CP radiation are demanded. In this context, one miniaturized dual-band CP conventional RDR is developed that achieves both characteristics (CP radiation and miniaturization) by the use of smaller metallic patches on all four sidewalls of the DR [31]. The $TE_{111}{}^y$ and $TE_{113}{}^y$ modes shifted towards lower frequency by 18.3% and 5.44% with respect to the baseline design. Additionally, the arrangement of metal patches excites the orthogonal modes to produce narrow 3 dB ARBWs are 3.64% and 1.37% at the lower and upper bands, respectively. Since the fields inside the CP DRAs rotate with the phase angle, the PEC boundary condition based volume reduction technique cannot be applied.

In this paper, we presented a size reduction of a dual-band CP DRA by exploiting the unconventional shape of the DR. The geometry of the DR is Y-shaped that has arms of unequal length and where the combination of linearly polarized E-field from different arms combine to produce CP radiation in the WLAN and WiMAX frequency bands [32]. By applying the PEC boundary on the longest arm, a size reduction with CP radiation is achieved but the required bands are not entirely covered. Therefore, some parameters are optimized and the final design achieved a size reduction of 33.18% with the 3 dB ARBWs fully incorporating the WLAN and WiMAX bands. A larger size reduction and wider 3 dB ARBWs are obtained as compared to [31]. The excited modes in the proposed design are identified by the Eigenmode simulations. The proposed design is fabricated and measured. The details of antenna design and size-reduction process, parametric study, Eigenmode analysis, and comparison of the simulated and experimental results are detailed in the following sections.

II. ANTENNA DESIGN

Fig. 1 shows the geometry of the miniaturized DRA. The DR is made up of Alumina ($\varepsilon_r = 10$) and placed on the upper side of a copper-backed Taconic RF-35 substrate ($\varepsilon_{sub} = 3.5$, $t = 1.52$ mm). The DR is excited through a strip that is vertically mounted on the Face-I of the DR. The dimensions of the feed were optimized to obtain better impedance matching at the desired frequencies. One arm of the DR is rotated by angle β and one of the faces namely Face-III is fully covered by the copper sheet to realize a PEC boundary. It can be seen that only a few parameters are shown in Fig. 1. A complete list of parameters is available in our previous study [32].

Fig. 2 depicts the design flow of the size-reduction and parameter optimization that is performed to cover the WLAN (2.401–2.495 GHz) and WiMAX (3.4–3.69 GHz) bands. The simulated results of the reflection coefficients and axial ratios (ARs) are plotted in Fig. 3. The geometry of the baseline design is from our earlier study [32] that obtains a wider -10 dB IBW of 62.07% (2.2–4.18 GHz). The generation of CP wave under 3 dB criterion is explained with the help

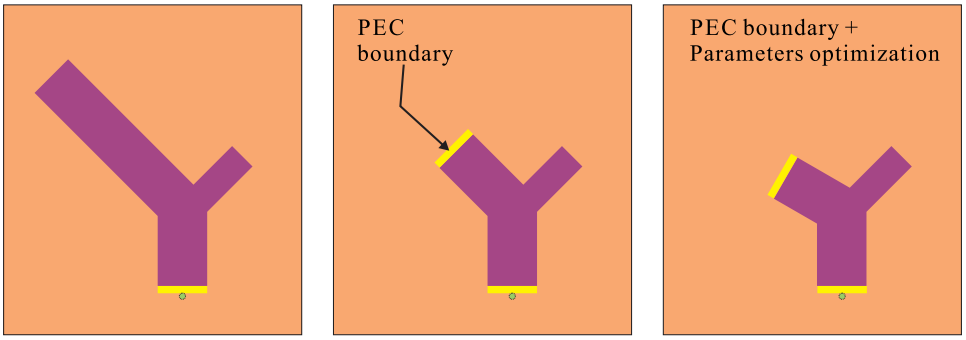

FIGURE 2. Design process of the proposed design.

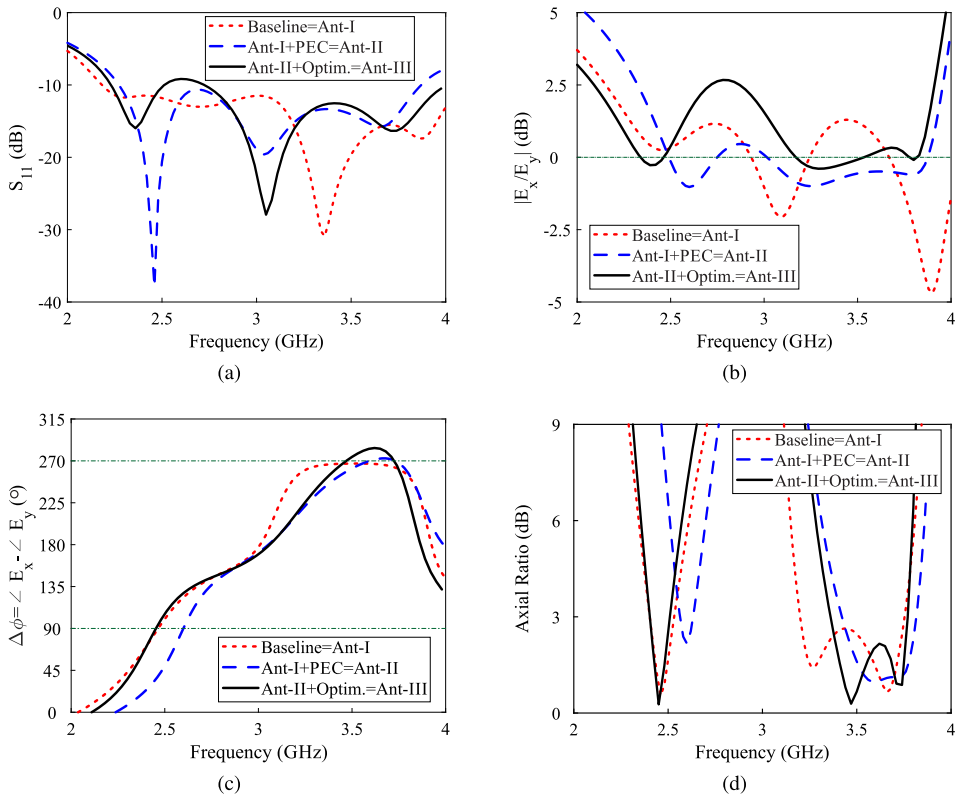

FIGURE 3. Comparison of the simulated results of the three antennas. (a) Reflection coefficients. (b) Amplitude ratios (E_x/E_y). (c) Phase differences ($\Delta\phi = \angle E_y - \angle E_x$). (d) Axial ratios.

of phase difference ($\Delta\phi$) and amplitude ratio (E_x/E_y) of the two orthogonal components ($\vec{E}_x$ and $\vec{E}_y$) of the E-field. The simulated results of E_x/E_y and $\Delta\phi$ for all three designs are plotted in Fig. 3(b) and (c), respectively. For the baseline design (Ant-I), the noted values from Fig. 3(b) and (c) are 0.37–0.43 dB/−(0.68–1.25 dB) and 70.39–108°/252.87–261.11°, respectively, to produce circular polarization in the frequency range of 2.4-2.53 GHz and 3.2–3.75 GHz. With the application of the PEC boundary on the long arm of Ant-I, a size reduction is achieved but −10 dB IBW is reduced to 52.12% (2.27–3.87 GHz). From Fig. 3(b), the E_x/E_y values for Ant-II exist within the limit at both bands, but the $\Delta\phi$ values in Fig. 3(c) do not meet the criteria around the WLAN band and 20 MHz of WiMAX band. The noted 3 dB ARBWs for Ant-II from Fig. 3(d) are 3.08% (2.56–2.64 GHz) and 10.79% (3.42–3.81 GHz). Therefore, some parameters (h, f_T, f_S, β) are optimized in Ant-II design and termed as Ant-III. From Fig. 3(a), a dual-band response is obtained with −10 dB IBWs of 11.81% (2.23–2.51 GHz) and 34.19% (2.74–3.87 GHz). It can be observed from Fig. 3(b) and (c) that the E_x/E_y and $\Delta\phi$ values are improved as compared to Ant-II, and the noted values

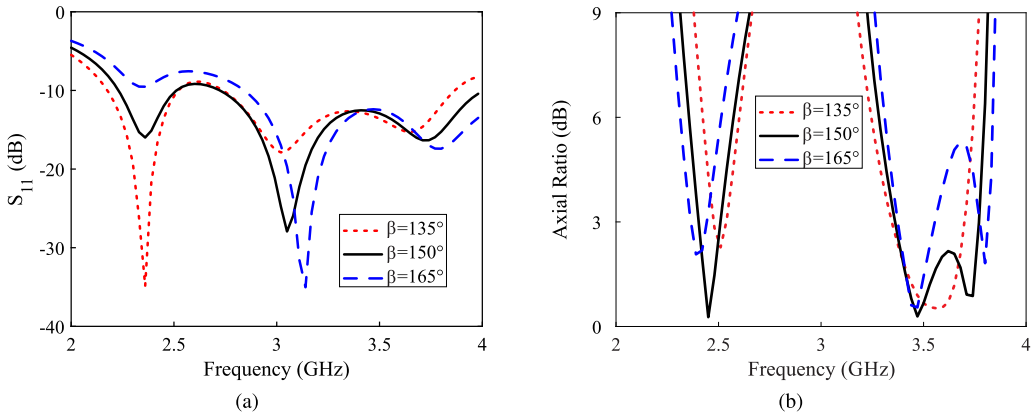

FIGURE 4. Simulated effects of change in rotation angle β of the miniaturized arm of the DR: (a) Reflection coefficients. (b) Axial ratios.

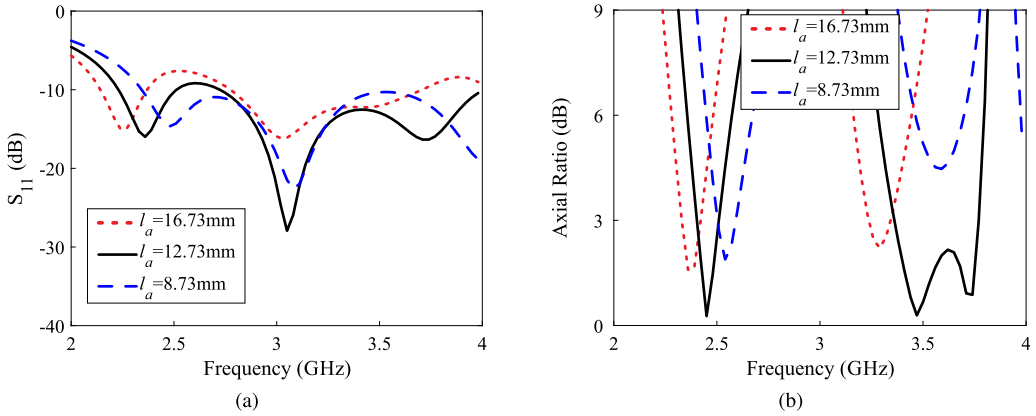

FIGURE 5. Simulated effects of change in length l_a of the miniaturized arm of the DR. (a) Reflection coefficients. (b) Axial ratios.

are −0.27–0.5 dB/ −0.35–0.04 dB and 69.82–108.56°/ 250.90–250.74°, respectively. The corresponding 3 dB ARBWs of the proposed design 4.48% (2.4–2.51 GHz) and 11.5% (3.36–3.77 GHz) that fully cover the frequency range WLAN and WiMAX bands, respectively. It can also be observed that the −10 dB IBWs and 3 dB ARBWs are narrower than the baseline design. Nonetheless, the total volume of the proposed DR is reduced as compared to the baseline design, and the frequency bands of interest are entirely covered. The volume reduction ($V_{red.}$) is calculated by

$$V_{red.}(\%) = \frac{V_{baseline} - V_{min.}}{V_{baseline}} \times 100 \quad (1)$$

where $V_{baseline} = 17517.21$ mm^3 is the volume of the baseline design and $V_{min.} = 11704.94$ mm^3 is the volume of miniaturized design. From (1), a volume reduction of 33.18% is achieved by the application of the PEC boundary.

III. PARAMETRIC STUDIES

Fig. 4 demonstrates the simulated effect of change in angle β of the miniaturized arm of the Y-shaped DR (YDR) on the reflection coefficients and ARs. It can be observed that the impedance matching at the lower band is predominantly affected by the angle β with an increase in the value of β. For the AR performance, the lower CP band tends to move towards the lower frequency side while the merged bands at the upper CP band tend to move away from one another with an increase in angle β. The best performance is achieved for $\beta = 150°$.

Fig. 5 shows the simulated effects of variations in length l_a of the miniaturized arm on the reflection coefficients and ARs. In the case of reflection coefficients, the resonance point of the lower band moves towards a lower frequency with an increase in the value of l_a. For the upper band, it can be observed that the resonance point around 3.75 GHz is mainly affected by changing l_a while the resonance point around 3 GHz remains almost constant. In the case of ARs, the upper band AR minimum at 3.7 GHz is significantly affected by the variations. The best response is noted for $l_a = 12.73$ mm.

Fig. 6 plots the simulated effects of changing the length l_b of the DR on the reflection coefficients and ARs. From Fig. 6(a), it can be observed that the resonance near 3 GHz shows a greater sensitivity to the change in length l_b. For ARs,

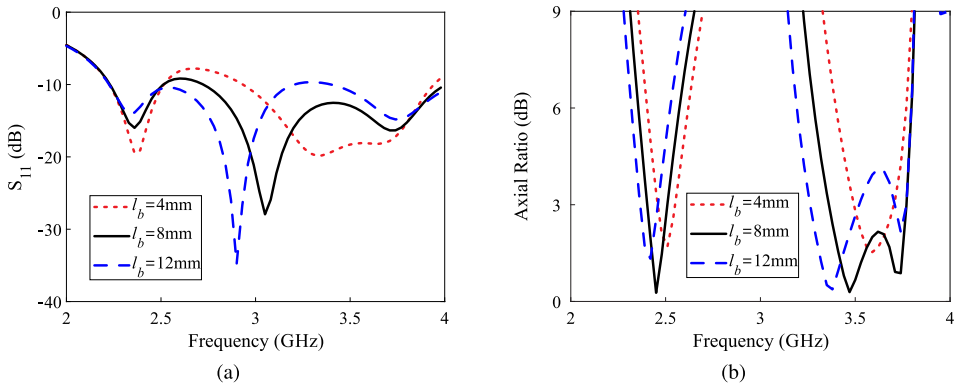

FIGURE 6. Simulated effects of change in length l_b of the DR. (a) Reflection coefficients. (b) Axial ratios.

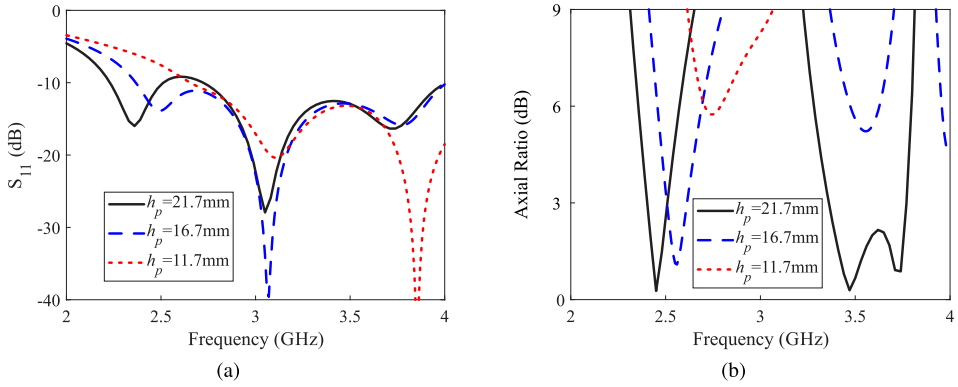

FIGURE 7. Simulated effects of change in length h_p of the PEC strip at Face-III. (a) Reflection coefficients. (b) Axial ratios.

the lower CP band is tuned as the length l_b is varied while the lower resonance in the upper CP band shows a greater variation as the length l_b is varied.

Fig. 7 depicts the simulated effects of change in length of the PEC at Face-III on the reflection coefficients and ARs. The length of PEC is represented by h_p and varies in a range of 21.7–11.7 mm with a stepsize of 5 mm. From Fig. 7(a), the lower band showed greater sensitivity to variations in h_p. From Fig. 7(b), the dual-band CP performance is achieved only for $h_p = 21.7$ mm.

IV. EIGENMODE ANALYSIS

Before performing the Eigenmode simulation, the simulated E-field at different frequencies are plotted for the proposed design as shown in Fig. 8. For the lower AR band, the simulated E-fields are observed on the top surface at 2.45 GHz for phase angles of $\angle 0°$ and $\angle 90°$ (see Fig. 8(a) and (b)). For the upper CP band, the fields are displayed in panoramic views at 3.05 GHz and 3.74 GHz as shown in Fig. 8(c) and (d). The angle of observation is selected for a clearer view of field distributions in the arm of length l_a and l_b. Afterward, an Eigenmode simulation of the proposed design is performed. From the Eigenmode simulation, four modes (Mode-1, Mode-2, Mode-3, and Mode-4) are identified that have the identical

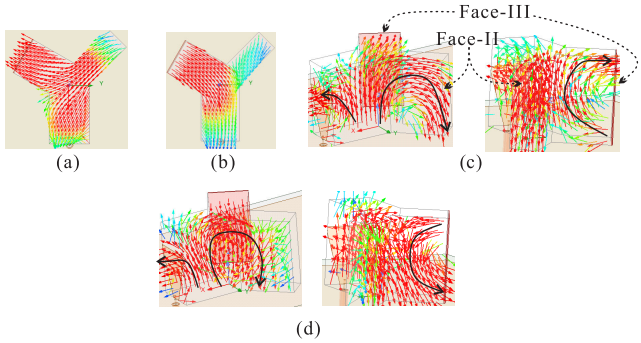

FIGURE 8. Simulated E-field distributions. (a) 2.45 GHz $\angle 0°$. (b) 2.45 GHz $\angle 90°$. (c) 3.05 GHz. (d) 3.74 GHz.

E-field distributions to those in Fig. 8. Fig. 9(a) plots the variations in resonance frequencies of these modes for change in the height h of the DR. For $h = 21.7$ mm, the resonance frequencies of these modes are also shown in Fig. 9(a) while the E-field distributions can be visualized in Fig. 9(b)–(e). It can be observed from Fig. 9(b) and (c) that the E-field distributions of Mode-I and Mode-II correspond to the dominant mode. The length of the resonant mode equals the sum of the length of the straight and miniaturized arm of the YDR

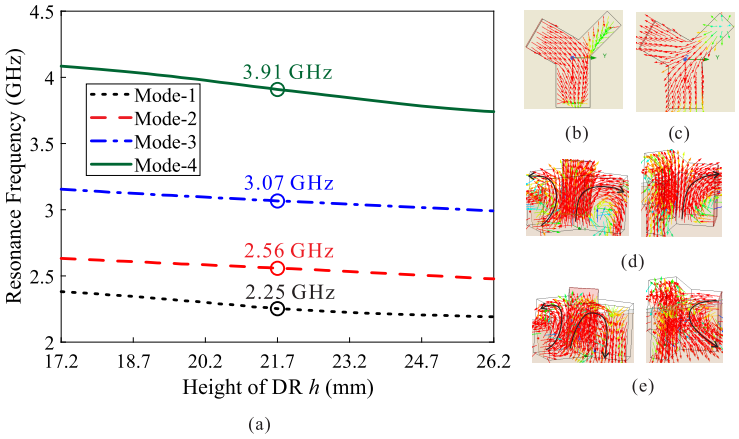

FIGURE 9. Eigenmode simulation. (a) Variations in resonance frequencies of Eigenmodes by altering the height of DR h. E-field distribution for $h = 21.7$mm of (b) Mode-1 at 2.25 GHz ∠0°, (c) Mode-2 at 2.56 GHz ∠180°, (d) Mode-3 at 3.07 GHz ∠180°, and (e) Mode-4 at 3.91 GHz ∠180°.

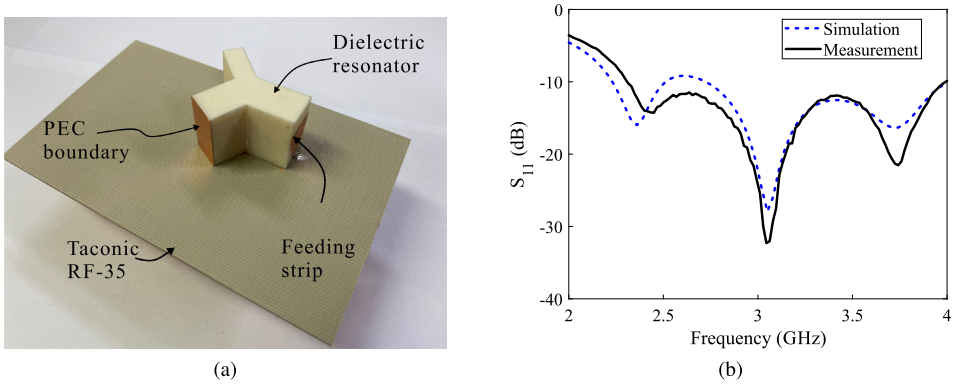

FIGURE 10. Fabricated prototype and measurement of the proposed design. (a) Photograph. (b) Comparative results of the simulated and measured reflection coefficients.

as the field is mostly concentrated in these two sections. By observing the left photos in Fig. 9(d) and (e), it is noted that the higher order modes are generated where the length of resonant modes is approximately one and a half wavelength. By comparing, it can be observed that the E-field distributions in Figs. 8(a) and 9(c), 8(b) and 9(b), 8(c) and 9(d), and 8(d) and 9(e) are similar. Also, the sense of circular polarization at both bands is already discussed in [32] and is not shown here to avoid repetition. The E-field distribution at the lower CP band in [32] is similar to Fig. 8(a) and (b) and demonstrates the generation of right-handed circular polarization (RHCP). Therefore, the application of the PEC boundary does not affect the polarity of the circular polarization. In addition, it is noted from Fig. 3(c) that the upper CP band is out of phase as compared to the lower band suggesting a reversal of polarity of the radiated CP wave, i.e., left-handed circular polarization (LHCP).

V. MEASUREMENT RESULTS AND DISCUSSION

A prototype of the proposed miniaturized CP DRA is fabricated and measured. Fig. 10 shows a photograph and comparative results of the reflection coefficients, where the measurement was performed using the Agilent E5071B RF network analyzer. From Fig. 10(b), a wide −10 dB IBW of 53.5% (2.3–3.98 GHz) is obtained in the measurement as compared to the dual-band response in the simulation. The deviation in the measured data can be related to the fabrication tolerances. Fig. 11(a) shows a photograph of the far-field testing of the fabricated prototype. The measurements were performed in the broadside direction ($\theta = 0°$, $\phi = 0°$) for two range of frequencies considering the simulated results. The comparison of simulated and measured 3 dB ARBWs and gains are depicted in Fig. 11(b). From the measured data, the 3 dB ARBWs of 4.08% (2.4–2.5 GHz) and 10.91% (3.38–3.77 GHz) were achieved as compared to simulated values of 4.48% (2.4–2.51 GHz) and 11.5% (3.36-3.77 GHz), respectively. The measured peak gains within the lower and upper CP bands are 4.83 dBic and 4.81 dBic, respectively. At the upper band, the maximum difference in the simulated and measured gain is 1.35 dB that is acceptable and can be attributed to misalignments in the measurement setup and tolerances in the fabrication and measurement [17].

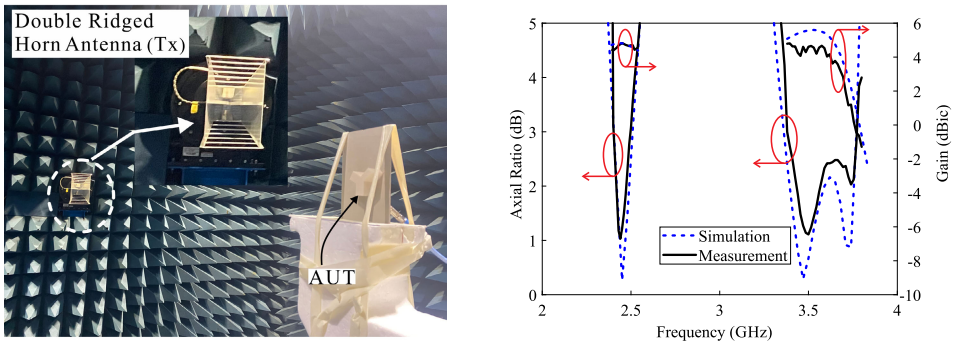

FIGURE 11. Comparison of the simulated and measured ARs versus frequency. (a) Photograph of the anechoic chamber. (b) Simulated and measured ARs and gains.

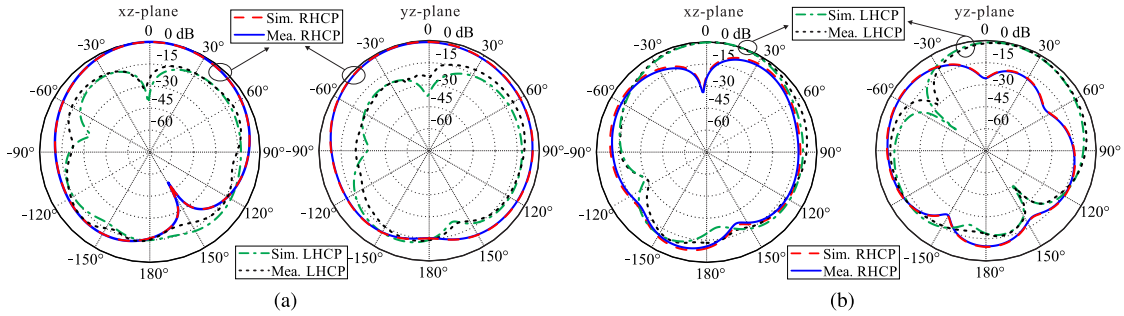

FIGURE 12. Simulated and measured radiation patterns of the proposed antenna in the *xz*- and *yz*-planes. (a) 2.45 GHz. (b) 3.5 GHz.

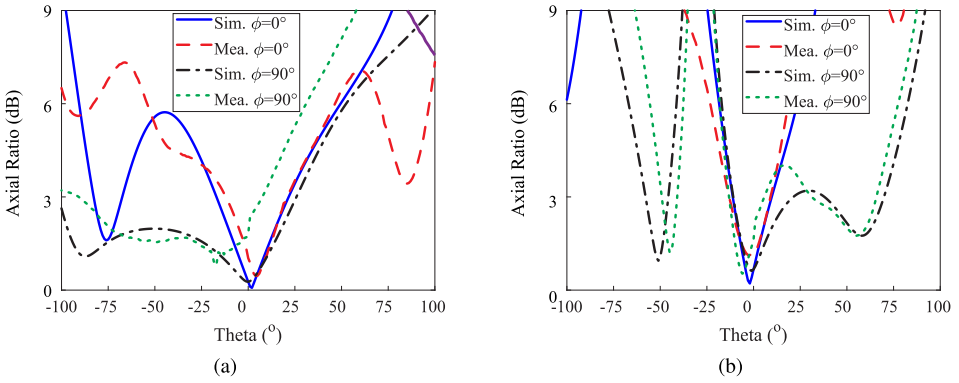

FIGURE 13. Comparison of the simulated and measured axial ratios versus theta in the *xz*-plane ($\phi = 0°$) and *yz*-plane ($\phi = 90°$). (a) 2.45 GHz. (b) 3.5 GHz.

The comparison of the simulated and measured CP radiation patterns at the frequencies of 2.45 GHz and 3.5 GHz for the *xz*- and *yz*-planes are depicted in Fig. 12. It can be observed that RHCP and LHCP radiation are dominant in the lower and upper CP bands, respectively. Moreover, the difference between the co- and cross-pol radiation in the broadside direction is greater than 23.5 dB for both frequencies. The mismatch between the simulated and measured results can be attributed to the measurement setup tolerances and misalignment between the antenna under test (AUT) and horn antenna. From the figure, the simulated/measured values of the front-to-back ratio for the broadside are 15.07/14.92 dB and 10.48/10.82 dB, respectively, that are similar to the earlier works [17], [33], [34].

Fig. 13 plots the graphs of simulated and measured ARs versus theta for the *xz*-plane ($\phi = 0°$) and *yz*-plane ($\phi = 90°$) at 2.45 and 3.5 GHz. From the plots, the simulated/measured 3 dB beamwidths at 2.45 GHz in the *xz*- and *yz*-planes are −17°–22° (39°)/−12°–21° (33°) and −102°–26° (128°)/−91°–8° (99°), respectively. Similarly, the values at 3.5 GHz are found to be −11°–10° (21°)/−13°–9° (20°) and −11°–22° (33°)/−6°–13° (19°) in the

TABLE 1. Performance comparison of the proposed miniaturized CP DRA with earlier works.

Ref.	Radiator	Miniaturization technique	Size reduction (%)	Radiated wave polarization	−10 dB IBW (%)	3 dB ARBW (%)	Gain (dBi/dBic)
[18]	Fan-blade-shaped DR	–	–	CP	17.47/28.94	13.33/7.81	3/<0
[32]	YDR	–	–	CP	62.07	4.92/12.64	4.11/6.48
[22]	Segmented DR	high ε_r	11.15	LP	17	–	5.5
[23]	CDR	PEC boundary	50	LP	5.3	–	–
[27]	RDR	Metal on the top and front wall	70	LP	10	–	5.7
[29]	RDR	AMC	85	LP	14.2	–	6.64
[30]	CDR	Slot with meandered lines	43	LP	18	–	0.8
[31]	RDR	Metal strips	18.32/5.44	CP	23.4/6.24	3.64/1.37	6.1/4.92
Prop.	YDR	PEC boundary	33.18	CP	53.5	4.08/10.91	4.83/4.81

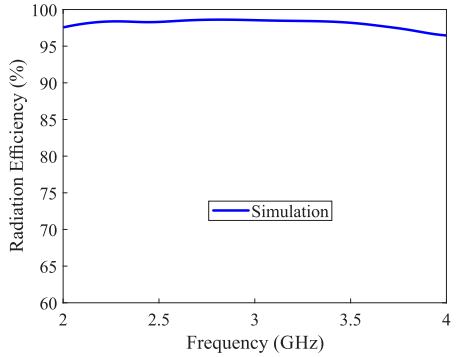

FIGURE 14. Simulated radiation efficiency of the proposed antenna.

xz- and *yz*-planes, respectively. From the graphs, there is a considerable difference in the results of the *yz*-plane that is mainly due to the misalignment between the Tx antenna and AUT as well as the tolerances in the measurement setup. Fig. 14 plots the simulated radiation efficiency of the proposed antenna that is greater than 97% within the 3 dB AR bands.

Table 1 summarizes a performance comparison of the proposed miniaturized CP DRA with some of the earlier studies [18], [22], [23], [27], [29]–[32]. In [18], a dual-band CP DRA is presented that has a wider 3 dB ARBW at the lower CP band. In comparison, the proposed work demonstrated a miniaturized design with a wider 3 dB ARBW at the upper band and higher peak gains at both bands. In our previous study [32], a YDR is presented that attains a wider −10 dB IBW and 3 dB ARBWs along with a higher gain at the upper band as compared to the proposed work. Nonetheless, the 3 dB ARBWs of the proposed work cover the whole frequency range of the intended applications using a radiator that is 33.18% smaller in volume. The DRAs in [22], [23], [27], and [29] are the miniaturized linear polarized (LP) antennas. In [22], segmented DRs with a top of higher ε_r than the lower one were utilized and one of the designs simultaneously achieved 11.15% miniaturization and 17% −10 dB IBW. The designs in [23] and [27] used pec boundary and metal wrapping to achieve a size reduction of 50% and 70% with −10 dB IBW of 5.3% and 10%, respectively. In [29], an AMC ground is applied to RDRA that achieves miniaturization of 85% and offers −10 dB IBW of 14.2%. Similarly, a meandered lines based slot fed CDRA achieves miniaturization of 43% with −10 dB IBW of 18%. Although the size reduction in the proposed design is less than the LP miniaturized designs, the antenna is a CP radiator and offers a wider −10 dB IBW. In [31], a miniaturized CP RDRA is presented where the application of metallic strips not only moves the resonance frequencies of the $TE_{111}{}^{y}$ and $TE_{113}{}^{y}$ modes by 18.32% and 5.44% at the lower and upper bands, respectively, but also creates degenerate modes. On the contrary, the CP in the proposed work is due to the shaped of the DR and a PEC boundary condition is applied to achieve a larger size reduction of 33.18%. In addition, the proposed work achieved a wider 3 dB ARBWs.

VI. CONCLUSION

In this paper, a PEC boundary condition is applied to achieve the size reduction of a dual-band circularly polarized (CP) Y-shaped dielectric resonator antenna (YDRA). A combination of the optimum location of a PEC boundary at the long arm of the dielectric resonator (DR) and the parameter optimization ensures a size reduction of 33.18% while maintaining a dual-band circular polarization response. The Eigenmode simulation is performed to identify resonance frequencies of modes of interest. The reflection coefficients of a prototype are measured using VNA showing −10 dB 53.5% (2.3–3.98 GHz). The far-field measurements demonstrated a 3 dB ARBWs of 4.08% (2.4–2.5 GHz) and 10.91% (3.38–3.77 GHz) that entirely cover the WLAN 2.4 GHz and WiMAX 3.5 GHz frequency bands. The proposed antenna can also be integrated with a 5G transceiver for the n78 band (3.4-3.7 GHz) that is auctioned in South Korea.

REFERENCES

[1] S. Long, M. McAllister, and L. C. Shen, "The resonant cylindrical dielectric cavity antenna," *IEEE Trans. Antennas Propag.*, vol. AP-31, no. 3, pp. 406–412, May 1983.
[2] M. W. McAllister, S. A. Long, and G. L. Conway, "Rectangular dielectric resonator antenna," *Electron. Lett.*, vol. 19, no. 6, pp. 218–219, Mar. 1983.
[3] M. W. McAllister and S. A. Long, "Resonant hemispherical dielectric antenna," *Electron. Lett.*, vol. 20, no. 16, pp. 657–659, Aug. 1984.

[4] K.-W. Khoo, Y.-X. Guo, and L. C. Ong, "Wideband circularly polarized dielectric resonator antenna," *IEEE Trans. Antennas Propag.*, vol. 55, no. 7, pp. 1929–1932, Jul. 2007.

[5] E. H. Lim, K. W. Leung, and X. S. Fang, "The compact circularly-polarized hollow rectangular dielectric resonator antenna with an underlaid quadrature coupler," *IEEE Trans. Antennas Propag.*, vol. 59, no. 1, pp. 288–293, Jan. 2011.

[6] R. Han, S. Zhong, and J. Liu, "Broadband circularly polarised dielectric resonator antenna fed by wideband switched line coupler," *Electron. Lett.*, vol. 50, no. 10, pp. 725–726, May 2014, doi: 10.1049/el.2014.0809.

[7] M. Elahi, A. Altaf, Y. Yang, K.-Y. Lee, and K. C. Hwang, "Circularly polarized dielectric resonator antenna with two annular vias," *IEEE Access*, vol. 9, pp. 41123–41128, 2021.

[8] C.-C. Lin and J.-S. Sun, "Circularly polarized dielectric resonator antenna fed by off-centered microstrip line for 2.4-GHz ISM band applications," *IEEE Antennas Wireless Propag. Lett.*, vol. 14, pp. 947–949, Dec. 2015.

[9] S. K. Khamas, "Circularly polarized dielectric resonator antenna excited by a conformal wire," *IEEE Antennas Wireless Propag. Lett.*, vol. 7, pp. 240–242, 2008.

[10] S. Fakhte, H. Oraizi, and R. Karimian, "A novel low-cost circularly polarized rotated stacked dielectric resonator antenna," *IEEE Antennas Wireless Propag. Lett.*, vol. 13, pp. 722–725, 2014.

[11] A. Ittipiboon, D. Roscoe, R. Mongia, and M. Cuhaci, "A circularly polarized dielectric guide antenna with a single slot feed," in *Proc. Symp. Antenna Technol. Appl. Electromagn. (ANTEM)*, Aug. 1994, pp. 427–430.

[12] X. Fang, K. W. Leung, and E. H. Lim, "Singly-fed dual-band circularly polarized dielectric resonator antenna," *IEEE Antennas Wireless Propag. Lett.*, vol. 13, pp. 995–998, 2014.

[13] A. Altaf, Y. Yang, K. Lee, and K. C. Hwang, "Circularly polarized Spidron fractal dielectric resonator antenna," *IEEE IEEE Antennas Wireless Propag. Lett.*, vol. 14, pp. 1806–1809, 2015.

[14] X. Wang, L. Sun, X. Lu, S. Liang, and W. Lu, "Single-feed dual-band circularly polarized dielectric resonator antenna for CNSS applications," *IEEE Trans. Antennas Propag.*, vol. 65, no. 8, pp. 4283–4287, Aug. 2017.

[15] A. Sharma, G. Das, and R. K. Gangwar, "Dual-band circularly polarized hybrid antenna for WLAN/WiMAX applications," *Microw. Opt. Technol. Lett.*, vol. 59, no. 10, pp. 2450–2457, Oct. 2017, doi: 10.1002/mop.30752.

[16] Y. D. Zhou, Y. C. Jiao, Z. B. Weng, and T. Ni, "A novel single-fed wide dual-band circularly polarized dielectric resonator antenna," *IEEE Antennas Wireless Propag. Lett.*, vol. 15, pp. 930–933, 2016.

[17] S. Trinh-Van, Y. Yang, K.-Y. Lee, and K. C. Hwang, "Single-fed circularly polarized dielectric resonator antenna with an enhanced axial ratio bandwidth and enhanced gain," *IEEE Access*, vol. 8, pp. 41045–41052, 2020.

[18] G. Varshney, V. S. Pandey, and R. S. Yaduvanshi, "Dual-band fan-blade-shaped circularly polarised dielectric resonator antenna," *IET Microw., Antennas Propag.*, vol. 11, no. 13, pp. 1868–1871, 2017.

[19] G. Varshney, S. Gotra, V. S. Pandey, and R. S. Yaduvanshi, "Inverted-sigmoid shaped multiband dielectric resonator antenna with dual-band circular polarization," *IEEE Trans. Antennas Propag.*, vol. 66, no. 4, pp. 2067–2072, Apr. 2018.

[20] M. Fallahpour and R. Zoughi, "Antenna miniaturization techniques: A review of topology- and material-based methods," *IEEE Antennas Propag. Mag.*, vol. 60, no. 1, pp. 38–50, Feb. 2018.

[21] R. K. Mongia and M. Cuhaci, "Low profile dielectric resonator antennas using a very high permittivity material," *Electron. Lett.*, vol. 30, no. 17, pp. 1362–1363, Aug. 1994, doi: 10.1049/el:19940924.

[22] A. Rashidian and D. M. Klymyshyn, "On the two segmented and high aspect ratio rectangular dielectric resonator antennas for bandwidth enhancement and miniaturization," *IEEE Trans. Antennas Propag.*, vol. 57, no. 9, pp. 2775–2780, Sep. 2009.

[23] M. Tam and R. D. Murch, "Half volume dielectric resonator antenna designs," *Electron. lett.*, vol. 33, no. 23, pp. 1914–1916, 1997.

[24] S. G. O'Keefe, S. P. Kingsley, and S. Saario, "FDTD simulation of radiation characteristics of half-volume HEM- and TE-mode dielectric resonator antennas," *IEEE Trans. Antennas Propag.*, vol. 50, no. 2, pp. 175–179, Feb. 2002.

[25] M. Boyuan, J. Pan, E. Wang, and D. Yang, "Miniaturized conformal arc dielectric resonator antennas using dielectric and metallic loading," *IEEE Access*, vol. 7, pp. 139518–139525, 2019.

[26] R. Mongia, "Reduced size metallized dielectric resonator antennas," in *IEEE Antennas Propag. Soc. Int. Symp. Dig.*, vol. 4, Jul. 1997, pp. 2202–2205.

[27] A. Rashidian and L. Shafai, "Compact lightweight polymeric-metallic resonator antennas using a new radiating mode," *IEEE Trans. Antennas Propag.*, vol. 64, no. 1, pp. 16–24, Jan. 2016.

[28] A. Rashidian, L. Shafai, and C. Shafai, "Miniaturized transparent metallodielectric resonator antennas integrated with amorphous silicon solar cells," *IEEE Trans. Antennas Propag.*, vol. 65, no. 5, pp. 2265–2275, May 2017.

[29] S. Khan, H. Ali, M. Khalily, S. U. A. Shah, J. U. R. Kazim, H. Ali, and C. Tanougast, "Miniaturization of dielectric resonator antenna by using artificial magnetic conductor surface," *IEEE Access*, vol. 8, pp. 68548–68558, 2020.

[30] N. Yang and K. W. Leung, "Size reduction of omnidirectional cylindrical dielectric resonator antenna using a magnetic aperture source," *IEEE Trans. Antennas Propag.*, vol. 68, no. 4, pp. 3248–3253, Apr. 2020.

[31] S. Gotra, G. Varshney, R. S. Yaduvanshi, and V. S. Pandey, "Dual-band circular polarisation generation technique with the miniaturisation of a rectangular dielectric resonator antenna," *IET Microw., Antennas Propag.*, vol. 13, no. 10, pp. 1742–1748, 2019.

[32] A. Altaf and M. Seo, "Dual-band circularly polarized dielectric resonator antenna for WLAN and Wimax applications," *Sensors*, vol. 20, no. 4, p. 1137, Feb. 2020. [Online]. Available: https://www.mdpi.com/1424-8220/20/4/1137

[33] M. Simeoni, R. Cicchetti, A. Yarovoy, and D. Caratelli, "Plastic-based supershaped dielectric resonator antennas for wide-band applications," *IEEE Trans. Antennas Propag.*, vol. 59, no. 12, pp. 4820–4825, Dec. 2011.

[34] S. Fakhte, H. Oraizi, R. Karimian, and R. Fakhte, "A new wideband circularly polarized stair-shaped dielectric resonator antenna," *IEEE Trans. Antennas Propag.*, vol. 63, no. 4, pp. 1828–1832, Apr. 2015.

AMIR ALTAF (Member, IEEE) received the B.S. degree in electrical engineering from the University of Engineering and Technology, Peshawar, Pakistan, in 2011, and the Ph.D. degree from the Division of Electronics and Electrical Engineering, Dongguk University, Seoul, South Korea, in 2018. He is currently working as a Postdoctoral Researcher with the Department of Electrical and Computer Engineering, Sungkyunkwan University, Suwon, South Korea. His research interests include circularly polarized antennas, reconfigurable dielectric resonator antennas, and development of millimeter-wave on-chip antennas and passive circuits. He is also a member of the IEEE Antennas and Propagation Society.

MUNKYO SEO (Senior Member, IEEE) received the B.S. and M.S. degrees in electronics engineering from Seoul National University, Seoul, South Korea, in 1994 and 1996, respectively, and the Ph.D. degree in electrical engineering from the University of California at Santa Barbara (UCSB), Santa Barbara, CA, USA, in 2007. From 1997 to 2002, he was an RF Engineer with LG Electronics Inc., Anyang, South Korea, designing microwave subsystems for wireless communication. From 2009 to 2013, he was with Teledyne Scientific Company, Thousand Oaks, CA, USA, where he worked on the design of various millimeter-wave, terahertz, and high-speed mixed-signal circuits. In 2013, he joined the Department of Electrical and Computer Engineering, Sungkyunkwan University, Suwon, South Korea, where he is currently an Associate Professor.